



A Vortex-Lattice Modeling Approach for Free-Surface Effects on Submerged Bodies and Propellers

Qiang Chen, Chen-Jun Yang^(✉), and Xiao-Qian Dong

State Key Laboratory of Ocean Engineering, Shanghai Jiao Tong University,
Shanghai 200240, China
cjyang@sjtu.edu.cn

Abstract. A vortex-lattice modeling approach is proposed for investigating the free-surface effects on the hydrodynamics of submerged moving bodies and the propeller in the frame of the potential flow theory. The bodies, the propeller, and the free surface waves generated by them are modeled uniformly by vortex lattices. By fulfilling simultaneously the non-penetration boundary condition on the body surface (or on the camber surface for a propeller) and the linearized free-surface boundary condition, a set of linear algebraic equations can be established and solved for the vortex strengths. The vortex lattices for modeling the body- or propeller-generated waves are located slightly above the still water surface, while those for modeling the body are located on the exact body surface. In the case of the propeller, the vortex-lattice lifting-surface model is employed at present and combined with the vortex-lattice free-surface model. A number of test cases are given to investigate the convergence property and accuracy of the proposed approach, in terms of body-surface velocity or pressure distributions, as well as the lift and the wave-making resistance. Then the free-surface effects on quasi-steady propeller hydrodynamics are simulated and investigated at different submerged depths.

Keywords: Potential flow theory · Vortex-lattice method · Free-surface effects · Hydrodynamics · Body · Propeller

1 Introduction

The free surface has an adverse effect on the hydrodynamic performance of submerged moving bodies and propellers. For example, when the shaft submergence is small, the thrust and torque of a propeller would decrease slightly as compared with those in the open water due to the wave-making effects. To evaluate the powering performance of a ship in waves more accurately, it is worthwhile to evaluate the free surface effects on propeller performance in addition to the hull resistance increase.

In 1978, Kerwin et al. [1] proposed the vortex-lattice modeling approach based on the lifting-surface theory for predicting the steady and unsteady performances of marine propellers. In this method, the propeller blades were replaced by a set of vortex lattices located on the camber surface, and the center of each vortex lattice is chosen as the control point where the non-penetration boundary condition is fulfilled. In the

1980s, the quasi-continuous method (QCM), which was proposed for thin wing problems by Lan [2], was introduced by Nakamura [3] to solve the steady flow problem of marine propellers, and extended to unsteady flow problems by Hoshino [4]. To make the method of Kerwin et al. [1] more practical, Wang et al. [5, 6] proposed their own wake model to prescribe the trailing vortex geometry, and validated the model against model test data for several propellers.

On the other hand, a number of potential-flow methods were proposed for investigating the free-surface effects on submerged moving bodies including the propeller. In 1994, a numerical lifting-line method was presented in [7] for the calculation of lift on a planar hydrofoil of finite span near the free surface, where the free-surface boundary condition was fulfilled by an image and the so-called wave-making velocity potential. In the next year, a vortex lattice method with the same free-surface boundary condition was presented in [8] to solve the same problem. In 1989, a vortex-lattice model was presented for the calculation of quasi-steady propeller hydrodynamics near the free surface in [9], and this model fulfilled non-penetration boundary condition, the linearized free-surface boundary condition and the Kutta condition. And the linearized free-surface boundary condition was fulfilled by adding the image and wave-making velocity potential, wherein the propeller was thought as approximately infinite blade to simplify the problem. In the same year, a numerical model based on boundary element method was presented in [10] to compute the wave resistance of submerged moving bodies and effects of the free surface were taken into account by an iterative procedure. Afterwards, a lot of research on the boundary element method was conducted by Bal et al. [11–17] for the problem of a hydrofoil moving under the free surface. In 1998, a potential-based panel method for 2-D hydrofoils without cavitation was presented in [11], where the hydrofoil was approximated with line panels which have constant source strength and constant doublet strength distributions and the free surface condition was linearized, satisfied by using the method of images. In [12], the interaction between the hydrofoil and the free surface was solved by iteration. In the same year, the free-surface boundary condition was extended to include the second-order effect in [13]. In the following year, this method was compared with other methods in [14]. In 2008, an iterative boundary element method was modified and extended to calculating the wave pattern and wave resistance of surface-piercing bodies, such as ship hulls and vertical struts [15]. Recently, the iterative boundary element method was extended to the case of two- and three-dimensional hydrofoils in water of finite depth [16] and the effects of free surface both on 2-D airfoils and 3-D wings moving steadily under the water surface were investigated in detail [17].

In this paper, a vortex-lattice model based on the potential flow theory is proposed for investigating the free surface effects on the hydrodynamic performance of submerged moving bodies and propellers. The vortex lattices for modeling the body are located on the exact body surface (or on the camber surface for a hydrofoil and a propeller) and those for modeling the body- or propeller-generated waves are located slightly above the still water surface. The control points for fulfilling the non-penetration boundary condition are located on the body surface (or on the camber surface) and those for fulfilling the linearized free-surface boundary condition are located on the still water surface. Then a set of linear algebraic equations can be

established and solved for the vortex strengths, and the hydrodynamic forces on submerged bodies or propellers can be evaluated.

2 Mathematical Formulation

The vortex-lattice method is based on the assumption that the fluid is inviscid and incompressible, and the flow is irrotational. As illustrated in Fig. 1, the body is submerged at a depth h_s beneath the still water surface, and experiences a steady uniform inflow along the x -axis. The total velocity potential can be expressed as

$$\Phi(x, y, z) = Ux + \phi(x, y, z) \quad (1)$$

where U and ϕ denote the uniform inflow velocity and the disturbance velocity potential due to the body, respectively. The disturbance velocity potential satisfies the Laplace equation,

$$\frac{\partial^2 \phi}{\partial x^2} + \frac{\partial^2 \phi}{\partial y^2} + \frac{\partial^2 \phi}{\partial z^2} = 0 \quad (2)$$

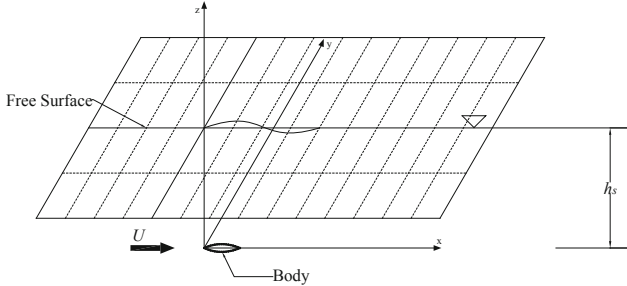


Fig. 1. Definition of coordinate system

The boundary conditions must be satisfied as follow:

- 1) Far from the body (and the trailing vortex sheets in the case of the propeller), the disturbance velocity potential diminishes to zero,

$$\phi \rightarrow 0 \text{ as } r \rightarrow \infty \quad (3)$$

- 2) The total velocity component normal to the body surface (or the camber surface) is zero,

$$(\mathbf{U} + \nabla \phi) \cdot \mathbf{n} = 0 \quad (4)$$

where \mathbf{n} is the normal vector to the body or camber surface.

- 3) For the hydrofoil and the propeller, the Kutta condition at the trailing edge should be satisfied, *i.e.*, the velocity at the trailing edge must be finite in magnitude,

$$|\nabla \phi| < \infty \quad (5)$$

- 4) For the hydrofoil and the propeller, the trailing vortex sheets/lines must be force-free,

$$\Delta p = p^+ - p^- = 0 \quad (6)$$

where Δp denotes the pressure jump across the trailing vortex sheet.

- 5) On the still water surface, the linearized free-surface boundary condition is fulfilled,

$$\frac{U^2}{g} \frac{\partial^2 \phi}{\partial x^2} + \frac{\partial \phi}{\partial z} = 0 \quad (z = h_s) \quad (7)$$

where g represents gravitational acceleration. The free surface elevation is expressed as,

$$\zeta = - \frac{U}{g} \frac{\partial \phi}{\partial x} \quad (8)$$

3 Numerical Method

3.1 Vortex Lattices and Control Points

As illustrated in Fig. 2, the vortex lattices for modeling the body- or propeller-generated waves are located slightly above the still water surface, while those for modeling the body or the propeller are located on the exact body surface or the camber surface. The control points for fulfilling the linearized free-surface boundary condition are located exactly on the still water surface, while those for fulfilling the non-penetration boundary condition are located on the exact body surface or the camber surface. In Fig. 2, the dh denotes the vertical distance from the free-surface vortex lattices to the still water surface. The body (or the camber surface of a propeller blade) and the free surface are discretized into M and N vortex lattices, respectively.

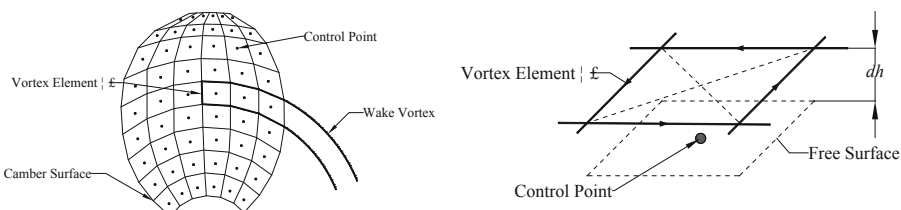


Fig. 2. Vortex lattices and control points for the propeller (left) and the free surface (right).

3.2 Non-penetration Boundary Condition on Body Surface

The non-penetration boundary condition, *i.e.* Eq. (4), can be expressed in discretized form as,

$$\sum_{k=1}^{M+N} \left[u_x^*(m, k) \cdot n_x + u_y^*(m, k) \cdot n_y + u_z^*(m, k) \cdot n_z \right] \cdot \Gamma_k = -U \cdot n_x \quad (1 \leq m \leq M) \quad (9)$$

where $u_x^*(m, k)$, $u_y^*(m, k)$ and $u_z^*(m, k)$ are the induced velocity coefficients, and (n_x, n_y, n_z) is the unit vector normal to the body or camber surface. The index m denotes the m^{th} control point on the body or camber surface.

3.3 Linearized Free-Surface Condition

Based on the induced velocity, the derivatives of ϕ in the linearized free-surface condition (7) is reduced by one order,

$$\frac{U^2}{g} \frac{\partial u_x(n)}{\partial x} + u_z(n) = 0 \quad (M+1 \leq n \leq M+N) \quad (10)$$

where $u_x(n)$ and $u_z(n)$ denote the x and z components of induced velocity at the n^{th} control point (on the free surface), respectively. The induced velocity components are expressed as

$$\nabla \phi = \left(\frac{\partial \phi}{\partial x}, \frac{\partial \phi}{\partial y}, \frac{\partial \phi}{\partial z} \right) = (u_x, u_y, u_z) \quad (11)$$

$$u_{x,y,z}(n) = \sum_{k=1}^{M+N} u_{x,y,z}^*(n, k) \cdot \Gamma_k \quad (M+1 \leq n \leq M+N) \quad (12)$$

The term $\partial u_x / \partial x$ in Eq. (10) is evaluated by a fourth-order upwind finite difference scheme [12]. As illustrated in Fig. 3, the derivative of u_x with respect to x at the i^{th} control point along the inflow direction is expressed as

$$\left(\frac{\partial u_x}{\partial x} \right)_i = C_i \cdot u_{x,i} + C_{i-1} \cdot u_{x,i-1} + C_{i-2} \cdot u_{x,i-2} + C_{i-3} \cdot u_{x,i-3} \quad (13)$$

where the coefficients C_i through C_{i-3} are determined by the fourth-order upwind finite difference scheme.

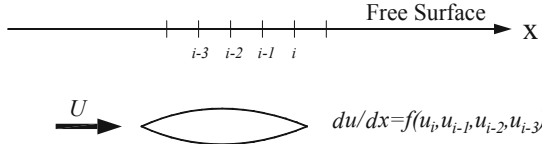


Fig. 3. Evaluation of velocity derivative by the fourth-order upwind finite difference scheme.

3.4 Linear Algebraic Equations

By combining (9) and (10), i.e. fulfilling the body-surface and free-surface boundary conditions simultaneously, a set of linear algebraic equations of order $M + N$ are obtained, where M equations are contributed from the body surface, and the rest from the free surface. The linear equations are written in matrix form as

$$\begin{pmatrix} a_{11} & \cdots & a_{1M} & a_{1,M+1} & \cdots & a_{1,M+N} \\ \vdots & \ddots & \vdots & \vdots & \ddots & \vdots \\ a_{M1} & \cdots & a_{MM} & a_{M,M+1} & \cdots & a_{M,M+N} \\ b_{11} & \cdots & b_{1M} & b_{1,M+1} & \cdots & b_{1,M+N} \\ \vdots & \ddots & \vdots & \vdots & \ddots & \vdots \\ b_{N1} & \cdots & b_{NM} & b_{N,M+1} & \cdots & b_{N,M+N} \end{pmatrix} \begin{pmatrix} \Gamma_1 \\ \vdots \\ \Gamma_M \\ \Gamma_{M+1} \\ \vdots \\ \Gamma_{M+N} \end{pmatrix} = \begin{pmatrix} c_1 \\ \vdots \\ c_M \\ 0 \\ \vdots \\ 0 \end{pmatrix} \quad (14)$$

In Eq. (14), the a_{ij} and c_i ($1 \leq i \leq M$, $1 \leq j \leq M + N$) correspond to Eq. (9), and the b_{mn} ($1 \leq m \leq N$, $1 \leq n \leq M + N$) correspond to Eq. (10). The Γ_i ($1 \leq i \leq M$) are the vortex strengths on the body surface or the camber surface, while Γ_n ($M + 1 \leq n \leq M + N$) are the vortex strengths on the free surface.

Once the vortex strengths are obtained by solving Eq. (14), the surface velocity and pressure distributions over the body surface or the camber surface can be evaluated. The lift and wave-making resistance (or propeller) can be evaluated by integrating the pressure distribution. For the propeller, the thrust and torque are evaluated according to the vortex lattice method [5]. The free surface elevation is evaluated via Eq. (8), where the $\partial\phi/\partial x$ is replaced with u_x .

4 Validation and Numerical Results

According to the numerical method described in the previous section, a number of FORTRAN codes have been developed for evaluating the free surface effects on the hydrodynamic forces acting upon the sphere, the hydrofoil, and the propeller, respectively. The convergence properties of the method are investigated, and some of the numerical results are validated against theoretical or experimental results.

4.1 Sphere

At first, the simple case of a moving sphere is given here to verify the feasibility of the proposed approach. The submerged depth h_s/D is 1.0, where D is the diameter of the sphere. The Froude number Fr is equal to 0.5774, where Fr is defined as

$$Fr = \frac{V_A}{\sqrt{gD}} \quad (15)$$

where V_A denotes the advance speed of the sphere (along negative x axis).

The computational domain and vortex lattices are shown in Fig. 4. Taking advantage of the symmetry of flow about the x - z plane, only half of the sphere and the free surface need to be calculated. The sphere surface is discretized into 40 lattices in x direction and 80 lattices along each circumference in x - z plane. The still water surface is $20D$ in x direction and $15D$ in y direction, and is discretized into rectangular lattices with varied spacing in x and y direction. The vortex-lattice size increases at a constant growth rate in y direction and negative x direction, but remains constant in positive x direction.

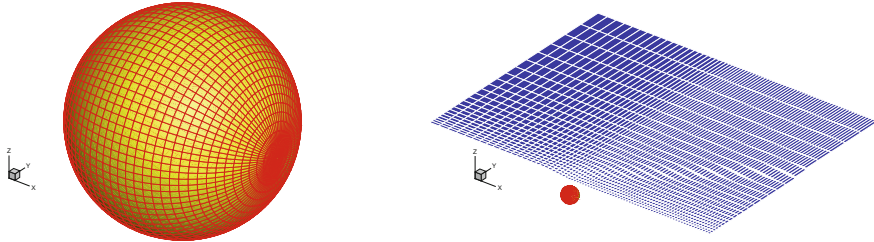


Fig. 4. Vortex lattices on sphere surface (left) and above the still water surface (right).

Since the vortex lattices are elevated above the still water surface by a height dh , it is essential that the results keep stable when dh is varied. Figure 5 shows the lift coefficient C_L , the wave-making resistance coefficient C_W , and the free surface elevation ζ (at $y = 0$) yielded from the present method using different dh values. It is clear that the said results are almost identical to each other for $0.075 \leq dh \leq 0.2$. However, no waves are generated numerically when $dh = 0$, which is because no horizontal velocity can be induced when the vortex lattices and control points are coplanar.

Secondly, the convergence property and accuracy of the proposed approach is investigated by changing the vortex-lattice size of the free surface while keeping that of the sphere unchanged. The computed results are compared with the theory ($C_L = 0.018$, $C_W = 0.0109$) in Table 1. It is clear that C_L and C_W both converge with ds , the minimum size of free-surface vortex lattices. The convergence of wave profile (ζ) with ds is shown in Fig. 6. In addition, the pressure distributions over the sphere surface without and with free surface are compared in Fig. 7.

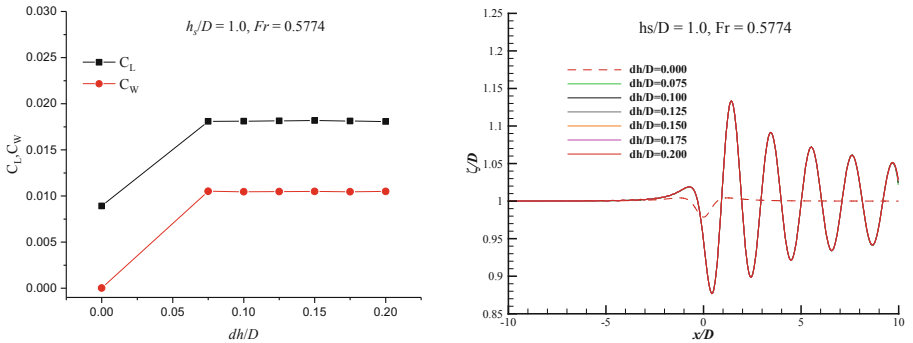


Fig. 5. The computed results of lift coefficient (C_L), wave-making resistance coefficient (C_W), and the free surface elevation ζ (at $y = 0$) at different elevated heights (dh) of the vortex lattices.

Table 1. Convergence of lift and wave-making resistance coefficients and the errors compared with theory.

ds/D	C_L	C_W
0.2	2.22%	-32.29%
0.15	1.06%	-14.40%
0.1	-0.06%	-4.95%
0.05	0.61%	-4.13%
0.04	0.33%	-5.23%

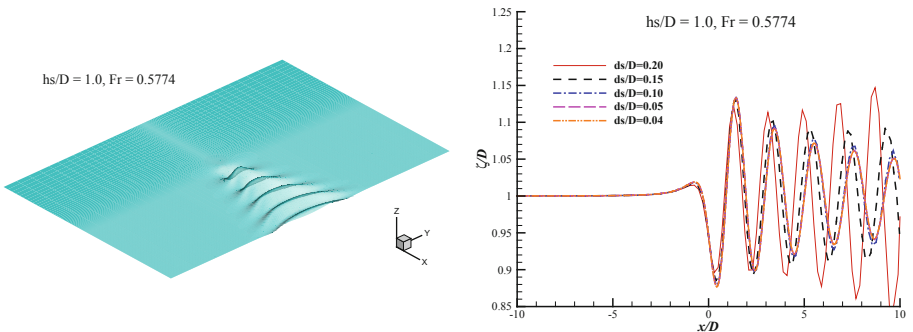


Fig. 6. Free surface wave profile (left) and the convergence of it with free-surface vortex lattice size (right), $Fr = 0.5774$.

Then, the VOF method is employed to simulate free surface effects on the sphere. The computational domain is a large cuboid, which is $20D$ in length, $20D$ in depth and width. The sphere is located at the center of the computational domain. As shown in Fig. 8, the meshes near the sphere and free surface are refined, unstructured meshes are used near the surface of sphere and structured meshes are used near the free surface and

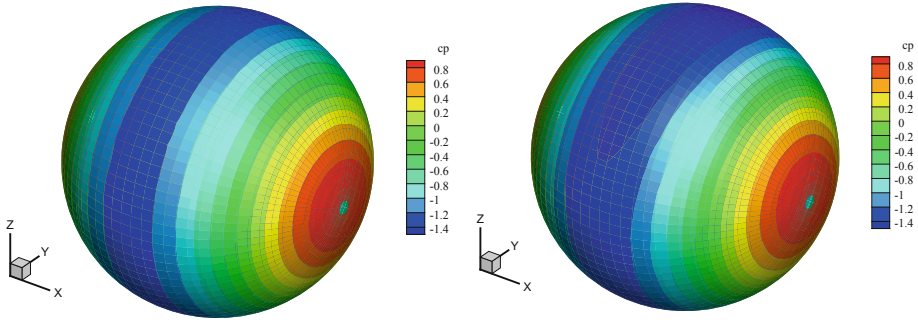


Fig. 7. The pressure distributions over the sphere surface without (left) and with (right) the free surface, $Fr = 0.5774$.

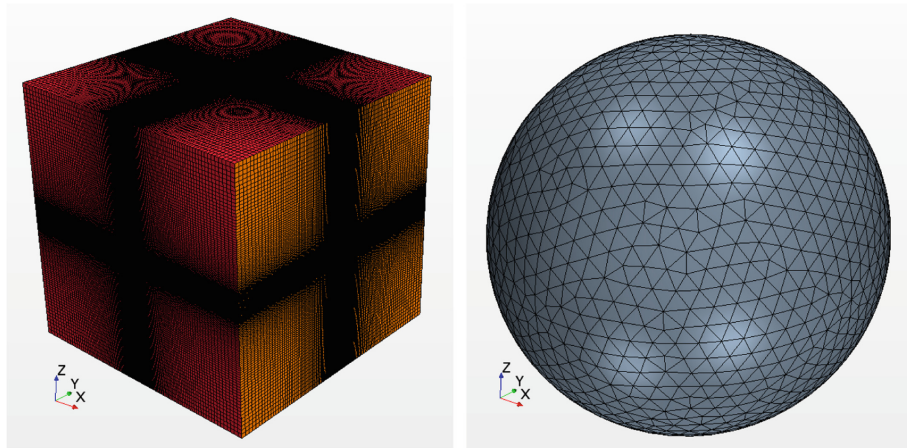


Fig. 8. Grids of the whole computational domain (left) and on sphere surface (right).

far away from sphere. The flow is assumed to be fully turbulent, and simulated by solving RANS equations and the standard $k-\varepsilon$ model via the SIMPLE scheme. The numerical simulations are conducted using the FLUENT software package.

Figure 9 compares the RANS and vortex lattice results of free surface elevations (ζ). It can be found that wave height by VOF method reduces much more rapidly than that simulated by the present method, but the first wave is relatively close to each other.

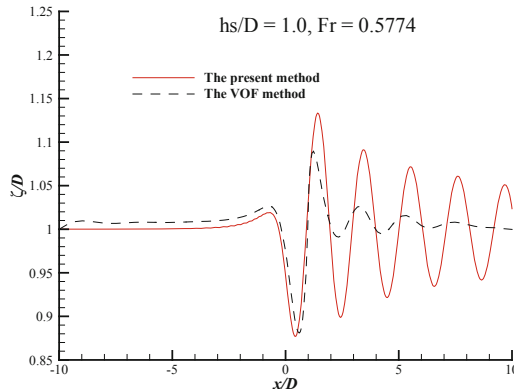


Fig. 9. Comparison of CFD and VLM simulated wave profiles.

4.2 Hydrofoil

The case of a rectangular hydrofoil moving along negative x axis is presented in this section. Its aspect ratio is 1.5, section camber line is NACA $a = 0.8$, and camber-to-chord ratio is 0.05. The submerged depth, h_s/c , is 1.0, where c denotes the chord length of the hydrofoil. The angle of attack, α , is 5° . The Froude number based on the chord length, $Fr = V_A/\sqrt{gc}$, is equal to 0.5774.

The computational domain and vortex lattices are shown in Fig. 10, where half of the foil and the free surface are calculated due to flow symmetry about the x - z plane. The hydrofoil surface is divided into 30 and 20 vortex lattices along the span and the chord, respectively. The free surface is $20c$ in x direction and $10c$ in y direction, where the arrangement of vortex lattices is similar to that in the case of the sphere. The trailing vortex wake lines are assumed to be straight and run parallel to the x axis.

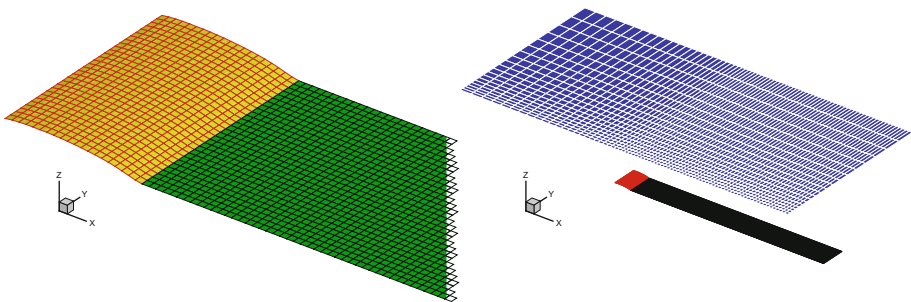


Fig. 10. Vortex lattices on the camber surface and wake surface of hydrofoil (left) and above the free surface (right).

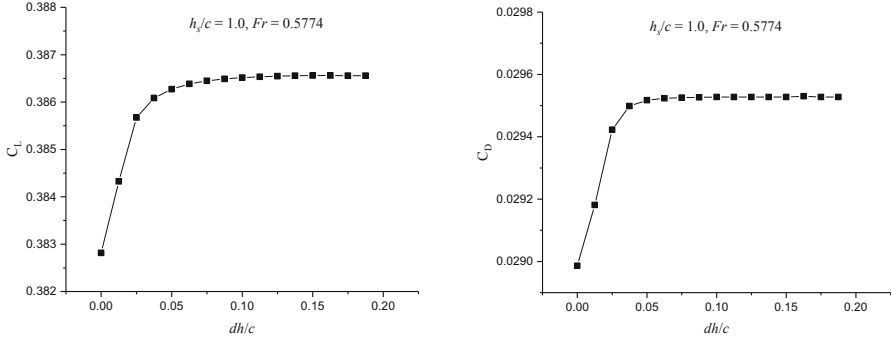


Fig. 11. The lift coefficient C_L (left) and drag coefficient C_D (right) calculated at different elevated heights (dh) of the vortex lattices.

Table 2. Convergence of lift and drag coefficients with free-surface vortex lattice size.

ds/c	C_L	C_D
0.20	0.386620	0.029550
0.15	0.386621	0.029541
0.10	0.386573	0.029530
0.05	0.386520	0.029530
0.03	0.386434	0.029526

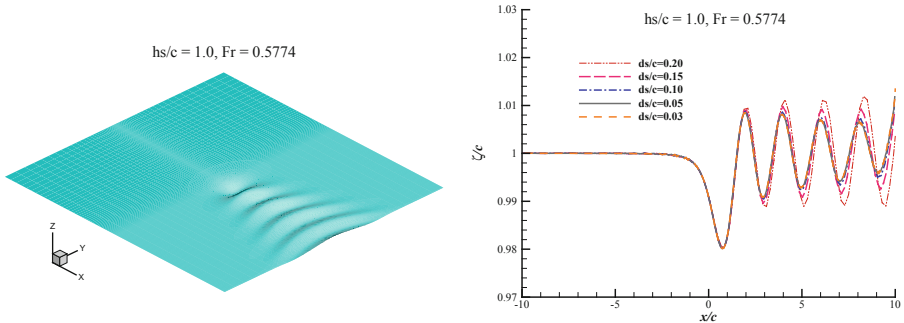


Fig. 12. Free surface profile (left) and convergence of it with free-surface vortex lattice size (right), $Fr = 0.5774$.

Firstly, the appropriate value of dh should be determined for subsequent calculations. According to the results shown in Fig. 11, $dh/c = 0.15$ is deemed as the appropriate value.

Secondly, the convergence property with free-surface vortex lattice size is presented in Table 2 and Fig. 12. It is seen that, in the case of the hydrofoil, the present vortex lattice model converges pretty fast as the vortex lattice size is reduced.

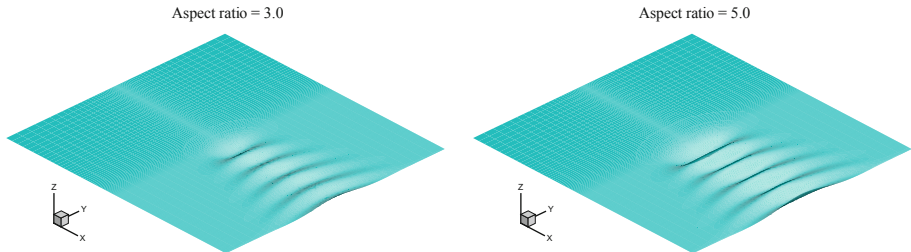


Fig. 13. Free surface profile, aspect ratios are 3.0 (left) and 5.0 (right), $Fr = 0.5774$.

In addition, two cases of different aspect ratios, 3.0 and 5.0, are presented. The wave profiles are shown in Fig. 13.

4.3 Propeller

The free-surface effects on the quasi-steady performance of a propeller are simulated with the proposed vortex lattice model, and investigated under different operating conditions. The series propeller, AU5-50, is selected for the investigation. Figure 14 shows the vortex lattice model, where the free surface is discretized in a way similar to that for the sphere and the hydrofoil, except that the symmetry of flow about the x - z plane no longer exists and the free surface is $20D$ in y direction. In addition to the advance coefficient $J = V_A/nD$, the Froude number, $Fr = V_A/\sqrt{gD}$, is another parameter which defines the working condition of the propeller. Here, $Fr \geq 1$ in most cases.

Firstly, it is necessary to determine an appropriate value for dh , the elevated height of free-surface vortex lattices. A number of pilot calculations are carried out using different values of dh , and the results are shown in Fig. 15 and Fig. 16 (left), where the submerged depth is $h_s/D = 0.6$. It can be found in Fig. 15 and Fig. 16 (left) that the results of K_T , K_Q and ζ keep stable when dh/D is within the range from 0.075 to 0.125, so 0.1 is selected as the appropriate value of dh/D for subsequent calculations.

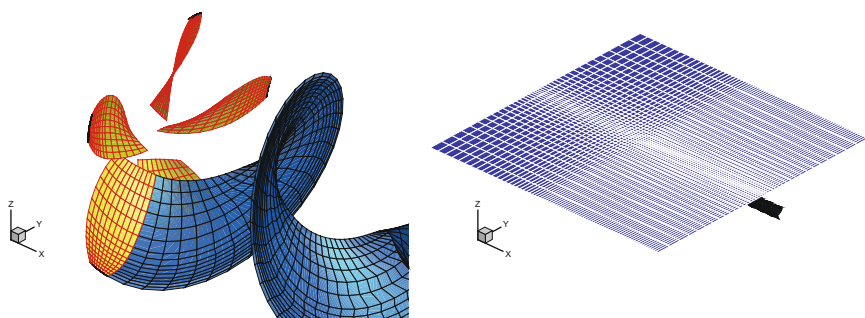


Fig. 14. Vortex-lattices on camber surface and wake surface of propeller (left) and them above free surface (right)

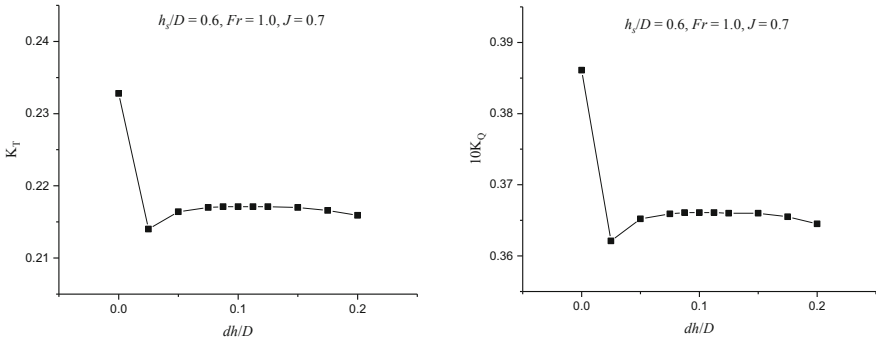


Fig. 15. Variations in propeller thrust (left) and torque (right) with dh , $Fr = 1.0$.

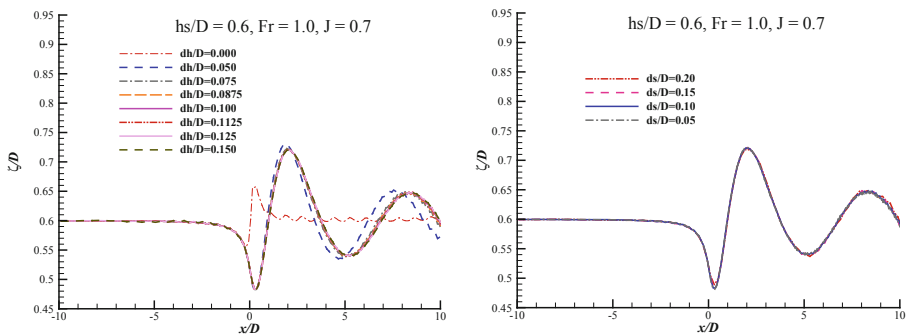


Fig. 16. Free surface profile with varying dh (left) and convergence of it with free-surface vortex-lattice size (right).

Secondly, the convergence of propeller thrust and torque and the wave elevation with the free-surface vortex lattice size is investigated, and the results are presented in Table 3 and Fig. 16 (right). It is shown that the influence of free-surface vortex lattice size is negligible.

Table 3. Convergence of hydrodynamic performance with free-surface vortex lattice size.

ds/D	K_T	$10K_Q$	η_o
0.20	0.2170	0.3660	0.6607
0.15	0.2171	0.3661	0.6607
0.10	0.2171	0.3661	0.6607
0.05	0.2171	0.3661	0.6607

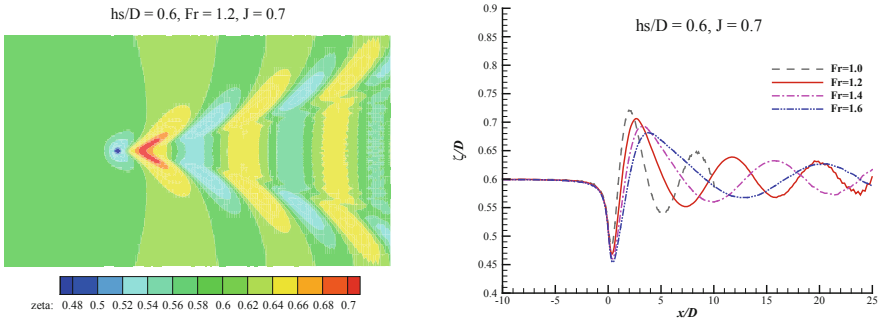


Fig. 17. Wave form at $Fr = 1.2$ (left) and free surface elevation with varying Froude number (right), $J = 0.7$, $h_s/D = 0.6$

The Froude number based on propeller diameter decreases with ship speed. Calculations are conducted at $Fr = 1.0, 1.2, 1.4$, and 1.6 to simulate different ship speeds. The advance coefficient J is set as 0.7 , and the submerged depth h_s/D is 0.6 . As shown in the Fig. 17 (left), the wave patterns generated by a propeller are similar to that by the bow of a ship. In Fig. 17 (right), it is shown that the transverse wavelength increases with the Froude number, at the same advance coefficient. When the Froude number increases, the influence of free surface on propeller thrust and torque decreases, as shown in Fig. 18.

The influence of shaft depth (h_s/D) is investigated here. In the calculation, there are three working conditions where the h_s/D is set to 0.6 , 0.8 , and 1.0 , respectively. The Froude number is set to 1.2 . The wave profile with varying shaft depths are presented in Fig. 19 (left). It is clear that the increase in shaft depth will decrease the free-surface effects on propeller performance.

In addition, the wave profiles with varying advance coefficients are shown in Fig. 19 (right). It can be found that, when the Froude number and the shaft depth are both kept unchanged, the wave height increases with the decrease in the advance coefficient.

In Fig. 20, the thrust and torque curves at different shaft depths are compared with those in the open water (deeply submerged) condition. It can be found that the free surface effects on propeller performance are more obvious when the advance coefficient and the shaft depth are smaller.

It is noted that the present method for the propeller with free surface tend to over-predict the thrust and torque when the shaft depth is too small or the propeller loading is too heavy. In those cases, air ventilation occurs and makes the thrust and torque drop drastically. Figure 21 shows an extreme condition where the propeller tip has emerged above the water surface.

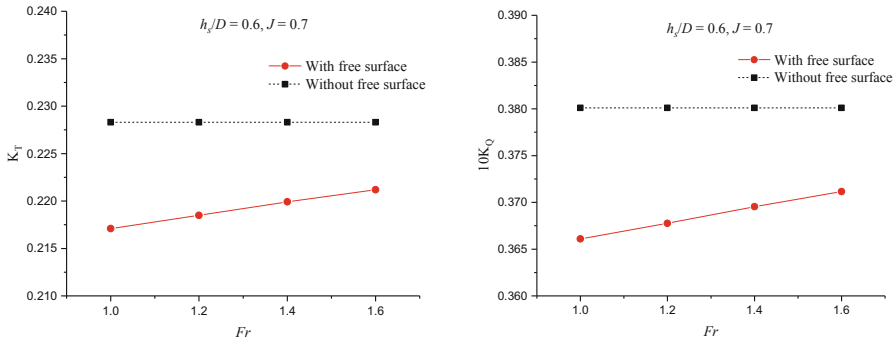


Fig. 18. The K_T (left) and $10K_Q$ (right) with varying Froude number, $J = 0.7$, $h_s/D = 0.6$.

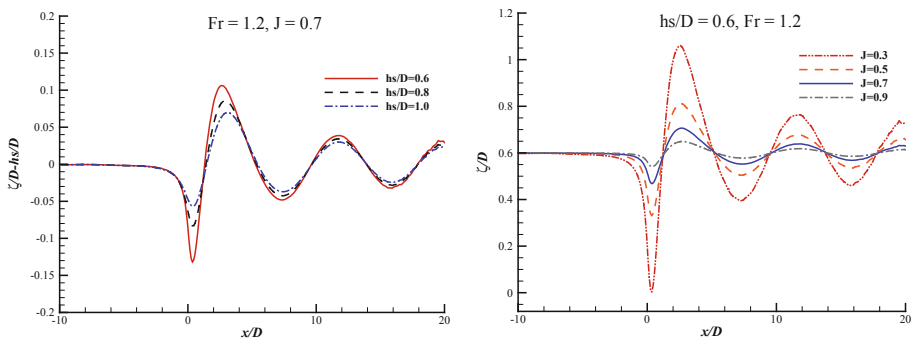


Fig. 19. Wave profiles with varying shaft depths (left) and them with varying advance coefficients (right), $Fr = 1.2$

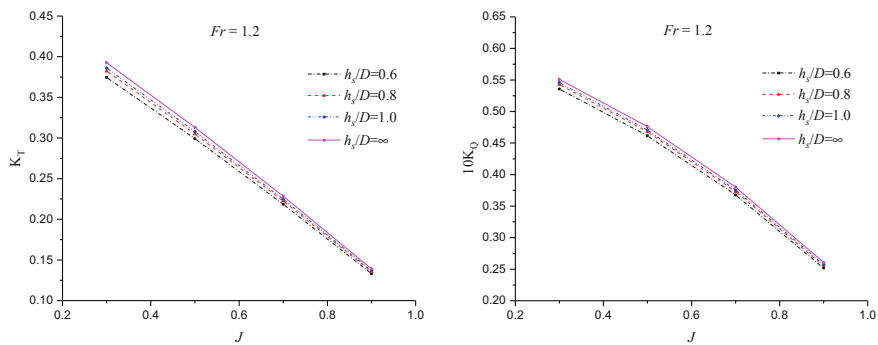


Fig. 20. Propeller thrust (left) and torque (right) coefficients at different shaft depths.

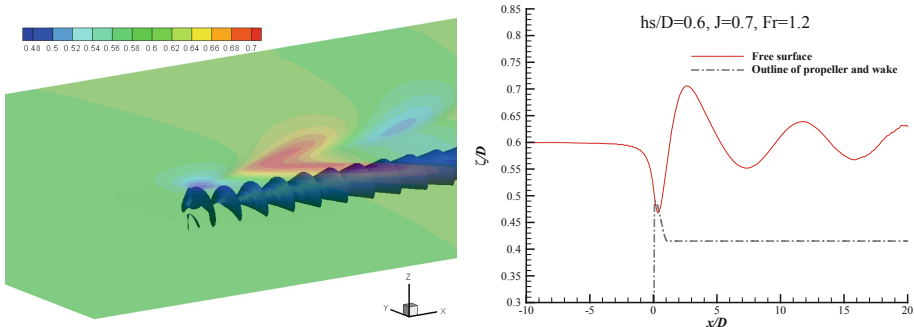


Fig. 21. Emergence of blade tip from water, $h_s/D = 0.6$, $J = 0.7$, $Fr = 1.2$.

5 Conclusion

In this paper, a vortex-lattice modeling approach based on the potential flow theory is proposed for simulating the free-surface effects on the hydrodynamics of submerged moving bodies and propellers. In this method, the body and the free surface are uniformly modeled by vortex lattices. The vortex lattices modeling the body- or propeller-generated waves are located slightly above the still water surface, while those modeling the body are located on the exact body surface. Several examples are given to verify the proposed approach. The following conclusions are drawn,

- 1) The proposed method converges fast and steadily with the decrease in free-surface vortex lattice size; and there exists a range of the elevated height of free-surface vortex lattices which ensures a reasonably accurate prediction of the free surface effect.
- 2) When the advance coefficient keeps unchanged, the decreases in propeller thrust and torque coefficients due to the free surface effect become smaller as the Froude number based on propeller diameter ($Fr = V_A/\sqrt{gD}$) increases, which means that the free surface effect becomes less important as the ship speed increases.
- 3) The influence of propeller shaft depth on propeller thrust and torque increases when the blade loading increases (*i.e.* the advance coefficient decreases).

As future work, the present vortex-lattice model will be extended to account for the unsteady propeller flow under the free surface.

References

1. Kerwin, J.E., Lee, C.S.: Prediction of steady and unsteady marine propeller performance by numerical lifting-surface theory. *Trans. SNAME* **86**, 218–253 (1978)
2. Lan, C.E.: A quasi-vortex-lattice method in thin wing theory. *J. Aircr.* **11**(9), 518–527 (1974)
3. Nakamura, N.: Estimation of propeller open-water characteristics based on quasi-continuous method. *J. Soc. Nav. Architects Jpn.* **1985**, 523–524 (1985)

4. Hoshino, T.: Application of quasi-continuous method to unsteady propeller lifting-surface problems. *J. Soc. Nav. Architects Jpn.* **1985**(158), 48–68 (1985)
5. Wang, G.Q., Hu, S.G., Yang, C.J.: Propeller analysis and design methods by numerical lifting surface theory. *J. Shanghai Jiaotong Univ.* **22**(2), 61–74 (1988). (In Chinese)
6. Wang, G.Q., Hu, S.G.: Improvement of prediction method of propeller characteristics and blade pressure distribution. *Shipbuild. China* **1**, 24–37 (1988). (in Chinese)
7. Thiart, G.D.: Numerical lifting line theory for a hydrofoil near a free surface. *S. Afr. Inst. Mech. Eng. Res. Dev. J.* **10**, 18–23 (1994)
8. Thiart, G.D.: Vortex lattice method for a straight hydrofoil near a free surface. *Int. Shipbuild. Prog.* **44**(437), 5–26 (1995)
9. Wang, G.Q., Jia, D.S.: Influence of free surface on propeller characteristics. *Shipbuild. Chin.* **1**, 1–8 (1989). (In Chinese)
10. Campana, E., Lalli, F., Bulgarelli, U.: A boundary element method for a non-linear free surface problem. *Int. J. Numer. Meth. Fluids* **9**(10), 1195–1206 (1989)
11. Bal, S.: A potential based panel method for 2-D hydrofoils. *Ocean Eng.* **26**(4), 343–361 (1998)
12. Bal, S., Kinnas, S.A., Lee, H.: Numerical analysis of 2-D and 3-D cavitating hydrofoils under a free surface. *J. Ship Res.* **45**(1), 34–49 (2001)
13. Bal, S.: Second-order free surface effect on cavitating 3-D hydrofoils. In: Proceedings of the ISOPE-2001 Symposium, Stavanger, Norway, pp. 554–561 (2001)
14. Bal, S., Kinnas, S.A.: A BEM for the prediction of free surface effects on cavitating hydrofoils. *Comput. Mech.* **28**(3–4), 260–274 (2002)
15. Bal, S.: Prediction of wave pattern and wave resistance of surface piercing bodies by a boundary element method. *Int. J. Numer. Meth. Fluids* **56**(3), 305–329 (2008)
16. Bal, S.: The effect of finite depth on 2D and 3D cavitating hydrofoils. *J. Mar. Sci. Technol.* **16**(2), 129–142 (2011)
17. Bal, S.: Free surface effects on 2-D airfoils and 3-D wings moving over water. *Ocean Syst. Eng.* **6**(3), 245–264 (2016)